Flux-flow noise in a $Pb_{0.8}In_{0.2}$ superconducting alloy

J. D. Thompson* and W. C. H. Joiner
Department of Physics, University of Cincinnati, Cincinnati, Ohio 45221
(Received 23 August 1978)

An investigation of flux-noise in $Pb_{0.8}In_{0.2}$ samples is presented. Good fits are obtained for experimental noise spectra using our recent model of fluxoid motion interrupted by pinning centers. A distribution of subpulse times is introduced in accordance with the model, and the data require that longer subpulse times be included when the samples undergo annealing which increases grain size. Since at *fixed* field the relative distribution of subpulse times does not shift with Lorentz force or fluxoid velocity, we conclude that pinning centers which are effective at interrupting fluxoid motion at one Lorentz force and fluxoid velocity appear to be effective at all forces and velocities in the linear flux-flow region. In our model, the noise at zero frequency, $W(0)$, is no longer simply proportional to the average intrinsic flux bundle size, but includes averages over distances between pinning centers. We refer to the appropriate new quantity as the generalized flux bundle size and we find that this quantity is affected by the sample metallurgy, increasing in proportion to grain size. The generalized flux bundle size also begins to decrease rapidly in the field vicinity of the volume pinning force maximum, and becomes small at H_{c2}. The data give an indication that there is a shift to shorter subpulse times in the region of the pinning force maximum. The concept of a "flux bundle" is discussed in light of the present results.

I. INTRODUCTION

After extensive studies, the static structures of fluxoids in type-II superconductors are now well understood.[1–3] The principal technique used in these studies is to obtain electron micrographs of ferromagnetic films evaporated onto the superconducting sample surface which replicate the fluxoid lattice.[1,2] Neutron diffraction has also been employed to study the static fluxoid lattice structure.[4,5]

Very little is known about the arrangement of fluxoids during flux motion. Although optical techniques have been employed to study the flow of multiply quantized flux structures in the intermediate state of type-I materials,[6] these cannot be employed in the type-II case because of the small size of the fluxoids. Recently, under special circumstances, neutron diffraction has been used to study certain aspects of the flux motion in a very pure sample.[7,8] However, it seems likely that the structures and processes involved in fluxoid motion, especially when this motion takes place in the presence of strong pinning interactions, will have to be inferred from other less direct observations. One such technique for studying flux motion is the measurement of the flux-flow noise spectrum, a technique first suggested by Van Ooijen and Van Gurp.[9] Despite several experimental and theoretical studies,[10–30] this suggestion has not led to a coherent picture of flux motion. In fact, much of the experimental work and the accompanying interpretations seem contradictory.

We believe that many of the experimental differences can be accounted for by the difference in the experimental procedures and arrangements. For example, in several instances[25,26] the experiments were performed in boiling liquid helium at 4.2 K, rather than below the liquid-helium λ point where bubble formation is suppressed. This is important since it has been shown that helium bubble formation is in itself a noise source which can mask the flux-flow noise.[10] We also believe that a more interesting reason for these differences is that the pinning sources were most likely markedly different in the various samples used. Since in the view which we will develop, these pinning sources determine the noise, the results represent real differences in the flux-flow characteristics of the samples examined. We find that in a general sense our results share a certain consistency with those of Van Gurp,[10] as well as results of Heiden,[17] when similar pinning characteristics are present.

In Sec. II, we review the results obtained from model calculations of the power spectrum. Section III describes our experimental procedure. Section IV deals with our experimental results which are summarized and discussed in Sec. V.

II. EXPRESSIONS FOR THE POWER SPECTRA

Moving fluxoids generate individual voltage pulses; thus, the time-dependent voltage along a sample in

which many fluxoids are moving can be written

$$V(t) = \langle V \rangle + \delta V(t) , \tag{1}$$

where $\langle V \rangle$ is the time-averaged or dc voltage, V_{dc}, given by $\nu\phi_0$, where ν represents the net rate at which fluxoids are moving across the sample, ϕ_0 is the flux quantum and $\delta V(t)$ is the time-dependent part of the voltage which derives from the discrete nature of the fluxoids and their motion across the sample. The noise power spectrum can be related to $\delta V(t)$. One defines the autocorrelation function for these voltage fluctuations as

$$\psi(T) = \langle \delta V(t) \delta V(t+T) \rangle . \tag{2}$$

Using the Wiener-Khintchine theorem,[31] the power spectrum, $W(f)$, is derived from the autocorrelation function by

$$W(f) = 4 \int_0^\infty \psi(T) (\cos 2\pi f T) dT . \tag{3}$$

Obviously the power spectrum will depend upon the voltage pulse shape generated by the moving fluxoids, as well as on the correlation between the pulses. The power spectrum may be written in the form

$$W(f) = W(0) G(f, f_c) , \tag{4}$$

where $W(0)$ can be shown to be proportional to the dc voltage $V_{dc} = \langle V \rangle$, and to be a function of the amount of flux contained in the "bundles" transiting the sample. The frequency dependence $G(f, f_c)$ is determined by the voltage pulse shape, and by the duration of the voltage pulses. Generally, this introduces a critical frequency, f_c, which is the inverse of the pulse duration, τ_c.

Early models[10–13] used to calculate the flux-flow noise spectrum have generally assumed that fluxoids move directly across the sample width, L, with constant velocity, v, and without interruption. If B is the magnetic induction, and d is the distance between voltage probes, $v = V_{dc}/Bd$, and

$$f_c = \frac{1}{\tau_c} = \frac{V_{dc}}{B\, dL} , \tag{5}$$

where τ_c is the transit time of the fluxoids across the sample width, L. The sample geometry and the voltage probe configuration have been shown to be important to the pulse shape.[11–13] For a narrow sample in which $2\pi d/L >> 1$, the voltage pulse generated by a fluxoid was originally found to be constant for the duration of its motion,[10,13] and the preceding considerations yield

$$W(f) = W(0) \left(\frac{\sin \pi f \tau_c}{\pi f \tau_c} \right)^2 . \tag{6}$$

Clem[29,30] has recently pointed out that his original calculation incorrectly accounted for the vector potential of the moving fluxoid, and has shown that for this geometry the voltage pulse shape should be

$$V = \frac{h v}{e} / [(\tfrac{1}{2} L)^2 - (vt)^2]^{1/2} \tag{7}$$

yielding a power spectrum

$$W(f) = W(0) J_0^2 (\pi f \tau_c) , \tag{8}$$

where J_0 is the zeroth-order Bessel function. The voltage pulse (7) varies slowly near the middle of the sample, but rises rapidly at the sample edges where flux enters and exists. The power spectra given by Eqs. (6) and (8) both oscillate with frequency. At high frequencies Eq. (6) decreases as $1/f^2$ whereas Eq. (8) decreases as $1/f$.

In the opposite geometric limit of $2\pi L/d >> 1$, Clem[12] has shown

$$W(f) = W(0) \left\{ \tfrac{1}{2} \exp - \left(\frac{2\pi f}{f_d} \right) + \frac{f_d}{4\pi f} \left[1 - \exp - \left(\frac{2\pi f}{f_d} \right) \right] \right\} . \tag{9}$$

In this latter case, the critical frequency is given by $f_d = v/d$, and is independent of sample width. In both instances

$$W(0) = 2\Phi V_{dc} , \tag{10}$$

where Φ represents the total flux in a bundle and is assumed to be the same for all bundles. The noise level can also be reduced by long-range correlation,[12] although the exact meaning and possible origins of this phenomenon have not been discussed.

In a previous note[21] we showed that in our samples satisfying $2\pi d/L >> 1$, the shape of the spectra was not given by Eq. (6), nor would it be given by Eq. (8). A better fit was obtained with the expression for the opposite geometric limit, Eq. (9), but the critical frequencies thus obtained were much higher than either f_c or f_d. We developed a model[21] in which fluxoid motion was interrupted for vanishingly short times by pinning centers, so that the original voltage pulse was divided into subpulses of duration τ_i. By assuming a power spectrum for the subpulses of the form given by Eq. (6) and integrating over an assumed distribution of subpulse times, we obtained both good fits to the experimental spectra and good agreement for values of f_c. Subsequently, we have shown that the assumption of zero stopping time is incorrect, and we have also corrected the form for the voltage subpulses.[23] We find

$$G(f, \tau_c) = \int_{\beta\tau_c}^{\alpha\tau_c} \left(\frac{\sin \pi f \tau_i}{\pi f \tau_i} \right)^2 g(\tau_i) d\tau_i , \tag{11}$$

where $g(\tau_i)$ is a distribution function for the τ_i's, and their limits are expressed in terms of τ_c, using

the parameters α and β. Also we find

$$W(0) = 2V_{dc}\frac{\langle\Phi^2\rangle\langle l^2\rangle}{\langle\Phi\rangle\langle l\rangle L}\ , \tag{12}$$

where $\langle\ \rangle$ represents an average over the sample and l is the distance traveled by a flux bundle before having its motion interrupted by a pinning center. The dc voltage then takes the form

$$V_{dc} = \frac{N\langle\Phi\rangle\langle l\rangle}{L}\ , \tag{13}$$

where N represents the pulse rate of all pulses generated by the moving fluxoids.

For samples having a low density of pinning centers, the majority of fluxoids will traverse the sample without having their motion interrupted, flux bundle size will be nearly uniform, and $W(0)$ as given by Eq. (12) will reduce to Eq. (10). In such a case

$$\langle l\rangle \cong \langle l^2\rangle^{1/2} \cong L\ , \tag{14}$$

which tends to increase the noise level. However, following the ideas which we will develop here, in these circumstances the concept of a flux bundle is not well defined, long-range correlation exists, and this may in turn produce an offsetting reduction in the noise.

In applying Eq. (11) to the calculation of the frequency dependence of the noise, it is necessary that we know the distribution function $g(\tau_i)$ for the subpulse times τ_i. We obviously have no *a priori* knowledge of this function. Moreover, different functional forms for $g(\tau_i)$ can lead to shapes for the power spectra which are quite similar, so that the form of $g(\tau_i)$ cannot be deduced from the spectrum shape. However, one general feature of $g(\tau_i)$ does influence the spectrum considerably. A preponderance of short pulses will produce a greater noise power at high frequencies, whereas a preponderance of long pulses will produce the opposite effect.

With these constraints in mind we have assumed the simplest form possible for $g(\tau_i)$, namely

$$\begin{aligned} g(\tau_i) &= \frac{1}{(\alpha-\beta)\tau_c}\ , \quad \alpha\tau_c \geq \tau_i \geq \beta\tau_c\ ; \\ g(\tau_i) &= 0\ , \quad \beta\tau_c \geq \tau_i\ , \quad \tau_i \geq \alpha\tau_c\ . \end{aligned} \tag{15}$$

In this case, α and β are treated as adjustable parameters which in a χ^2 minimization curve fitting procedure yield best fits to the data. From values of α and β thus obtained, we are able to make qualitative conclusions about the general distribution of τ_i's, or at least about the presence or absence of very short or very long pulse times.

Integrating Eq. (11) with this form for $g(\tau_i)$ we obtain

$$W(f) = \frac{W(0)}{\alpha-\beta}\left[\frac{\mathrm{Si}(2\pi f\alpha\tau_c)}{\pi f\tau_c} - \frac{\mathrm{Si}(2\pi f\beta\tau_c)}{\pi f\tau_c} + \frac{1}{\beta}\left[\frac{\sin(\pi f\beta\tau_c)}{\pi f\tau_c}\right]^2 - \frac{1}{\alpha}\left[\frac{\sin(\pi f\alpha\tau_c)}{\pi f\tau_c}\right]^2\right], \tag{16}$$

where $\mathrm{Si}(x) \equiv \int_0^x [(\sin u)/u]\,du$.

At the time of our formulation of this model, the corrected pulse shape calculated by Clem[29,30] was not available, and as noted, we used a square subpulse. Equation (7), corrected for the local velocity of each flux group, should therefore form the envelope for our subpulses. Although in principle we could include this correction in our model, the mathematics becomes intractible. We do not believe our use of square subpulses leads to substantial error. We justify this statement by noting that all our measured spectra, displaying a variety of shapes, can be fit quite closely to Eq. (16). This may be due to the fact that the majority of subpulses occurring away from the sample edges are reasonably flat, even on the basis of Eq. (7). As we will discuss subsequently, experimental spectra are relatively unchanged when the voltage probes are moved from the sample edges to the middle of the sample. If the high-frequency behavior of the measured spectra were determined by the rise in the pulse at the sample edges, one would expect these spectra to be altered. The fact that no alteration is observed may indicate that the high-frequency behavior, at least in the frequency range of our measurement, is determined by the duration of the shortest subpulses, rather than by the subpulse rise at the sample edges. It should be noted that an additional high-frequency contribution coming from motion at the sample edges could not be separated in our analysis from an alteration in the subpulse distribution function, $g(\tau_i)$, at short times. Neither the data presented here nor data taken under other experimental conditions suggests the need to account for additional high-frequency noise above that described by square pulses, and a $g(\tau_i)$ which is constant between the limits $\beta\tau_c$ and $\alpha\tau_c$.

III. EXPERIMENTAL PROCEDURE

A. Sample preparation

All samples to be discussed here were in the shape of foils with approximate dimensions $5 \times 0.4 \times 0.02$ cm. Exact dimensions for each sample are given in Table I. The composition of all samples was 80 at. %

Pb and 20 at.% In. The starting materials, Cominco 59 grade lead and indium, were melted in a quartz tube under a vacuum of approximately 10^{-6} Torr while being agitated by an external vibrator. After a 24 hour period, the tube containing the molten liquid was quenched into liquid nitrogen. The quartz tube was removed from the resulting ingot by a hydrofluoric acid etch. The ingot was then rolled to a thickness about ten times the final desired dimension. A piece of the ingot was cut from the rolled sheet so that in the final sample the direction of flux motion would be approximately parallel to the rolling direction. This piece of ingot was then inserted between glass microscope slides and placed in a hydraulic press where it was pressed to its final thickness. The thickness of the final sample varied less than ±5% over the sample length.

Samples were measured in one of three conditions: (i) as pressed, (ii) after etching the surface, or (iii) after annealing near the melting point. Surface etching was accomplished by immersing the sample in a solution of 20% hydrogen peroxide by volume in acetic acid for a period of approximately one minute, followed by a thorough rinsing with distilled water. Samples which were annealed were first given a light surface etch with concentrated nitric acid. Annealing was accomplished under a vacuum of 10^6 Torr at approximately 260 °C, for a period of one week. Following the anneal, the sample was cooled slowly, and etched in the acetic acid-hydrogen peroxide solution. Relevant sample information is listed in Table I.

B. Noise measurement

Each sample was mounted in a special holder designed to prevent any stresses which might otherwise arise because of temperature change. The magnetic field was applied perpendicular to the broad face of the sample and to the transport current which was parallel to the sample's long dimension. Current was introduced to the sample through thick copper clamps located at the sample ends. Voltage contacts were provided by spring loaded leads with conical ends maintained perpendicular to the sample surface to a height of 0.64 cm. The radius of contact of the most generally used leads was estimated to be 0.23 ±0.06 mm. All measurements were taken below the helium λ point at 2.14 K in order to eliminate flicker noise caused by helium bubble formation on the surface. Since the critical temperature for this alloy has been found to be $T_c = 6.91$ K, the temperature of measurement corresponds to a reduced temperature of

TABLE I. Sample dimensions, lead configuration and metallurgical condition.

Sample	d (cm)[a]	L (cm)[b]	t (cm)[c]	Metallurgical condition	Lead configuration[d]
6*d*	2.38	0.414	0.028	as pressed	normal lead configuration
6*de*	2.26	0.414	0.024	6*d* after etching	normal lead configuration
6*dea*	1.98	0.397	0.024	6*de* after annealing at 260 °C & light etching	normal lead configuration
6*ne*	2.10	0.198	0.020	as pressed & etched	normal lead configuration
6*new*	1.13	0.198	0.020	same as 6*ne*	wide voltage contacts[e]
6*we*	2.14	0.794	0.029	as pressed & etched	normal lead configuration
6*wec*	2.14	0.794	0.029	same as *we*	normal leads, but placed on center line of sample
6*te*2	2.38	0.397	0.056	as pressed & etched	normal lead configuration
6*tea*	2.22	0.397	0.056	annealed at 260 °C and lightly etched	normal lead configuration

[a] d : distance between voltage contacts.

[b] L : sample width.

[c] t : sample thickness.

[d] For normal lead configuration, voltage leads are placed parallel to long dimension of the sample, near sample edge, and narrow contacts are used ($r = 0.23$ mm).

[e] Wide contacts ($r = 0.89$ mm) are used in normal lead configuration.

$t = T/T_c = 0.310$. H_{c2} was found for each sample from a plot of critical current versus field, with the field oriented parallel to the surface. At 2.14 K, H_{c2} for the various samples was 5300 ± 140 Oe.

Considerable care was taken to shield the sample, the leads to the sample, and the low noise amplifiers which amplified the noise voltage signals. The sample itself was surrounded by a 1-cm-thick high-conductivity copper can, and voltage leads extending into the magnetic field region were rigidly mounted. Without such precautions, microphonics resulting from the liquid-nitrogen bubbling could generate signals much larger than the noise signals.

We also found it essential to use a current supply which was not ac powered. The current was therefore supplied by a bank of 12-V storage batteries, with a current output which was regulated so as to be stable during a run. Similarly our noise signal was amplified by two battery operated Keithly model 824 nanovolt amplifiers, providing a fixed gain of 120 dB. The amplified signal was measured with a General Radio model 1900-*A* wave analyzer. This instrument measures the voltage within a 3 cycle bandwidth, and the center frequency, using our calibration procedures, could, at frequencies below 100 cycles, be adjusted accurately to within ±1 cycle. The time constant of the instrument was adjusted so that the noise signal at a given frequency would be averaged over 30 seconds. Despite the precautions taken, as described above, occasional external noise bursts would enter the system. We would thus monitor the signal input with an oscilloscope, or the wave analyzer output with a digital voltmeter, while readings were being taken. When such noise bursts were observed, we would wait at least two time constants after their disappearance before taking a final reading. The frequency and amplitude response of the entire system was calibrated, and the 3 cycle effective bandwidth of the analyzer was verified. With these precautions we can normally resolve mean-square flux-flow noise voltages as small as 2×10^{-19} volt^2.

At a given frequency the mean-square flux-flow noise voltage is given by the difference of the squares of the root-mean-square noise voltage with the transport current on and with it off. Thus, the background is subtracted with the same magnetic field present as for the signal. This tends to eliminate any remaining extraneous signal due to microphonics. For a typical spectrum, 20 or more points are taken covering the frequency range of interest. The measurement of a spectrum takes approximately an hour, and only two, or at most three, spectra can be taken in a single run. For this reason, when we wished to know only $W(0)$ as a function of some parameter, we would often take the noise power at only a single frequency, typically 10 Hz, as that parameter was varied.

IV. EXPERIMENTAL RESULTS

A. Shape of the flux-flow noise power spectra and distribution of subpulse times

Three typical spectra are shown in Fig. 1 for samples 6*de* ($V_{dc} = 500$ uV), 6*dea* ($V_{dc} = 3000$ uV), and 6*ne* ($V_{dc} = 100$ uV). The field in each case is

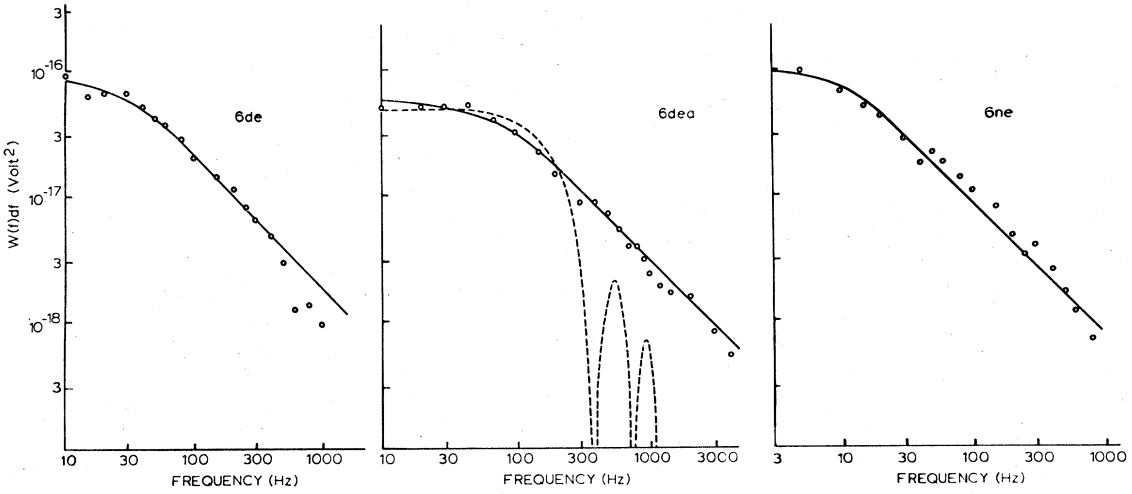

FIG. 1. Flux-flow noise power spectra for samples 6*de*, 6*dea*, and 6*ne*. Spectra are taken in each case at $T = 2.14$ K, $H = 3200$ Oe. For 6*de*, $V_{dc} = 500$ μV; for 6*dea*, $V_{dc} = 3000$ μV and for 6*ne*, $V_{dc} = 100$ μV. The solid curves represent both a χ^2 minimization fit to Eq. (9) yielding f_d^{fit} values of: 226 Hz (6*d*), 630 Hz (6*dea*), and 86 Hz (6*ne*), and an indistinguishable χ^2 minimization fit to Eq. (16) with $\beta = 0$, $\alpha = 1$, yielding f_c^{fit} values of: 42 Hz (6*d*), 117 Hz (6*dea*), and 15 Hz (6*ne*). For 6*dea* we also show as a dashed curve a χ^2 minimization fit to Eq. (6). This fit leads to a critical frequency of 374 Hz and is obviously a poor representation of the data.

TABLE II. Calculated and experimental critical frequencies for spectra shown in Fig. 1.

Sample	f_d^{calc} (Hz)	f_c^{calc} (Hz)	f_d^{fit} (Hz)	f_c^{fit} (Hz)	α
6*de*	3.1	17.6	226	42	0.4
6*dea*	23.9	119.3	630	117	1.0
6*ne*	0.7	7.5	85.6	15	0.5

$H = 3200$ Oe. The ratio $2\pi d/L = 34.3$ (6*de*), 31.3 (6*dea*), 66.6 (6*ne*) for the three samples, and thus for uninterrupted flux motion the spectrum should be given by Eq. (6) (square pulse) or by Eq. (8). However, the oscillatory behavior predicted by Eqs. (6) or (8) is not observed in the data. For example, in Fig. 1, we have used a χ^2 minimization program to obtain the best fit to Eq. (6) to our data for sample 6*dea*, and this is shown as the dashed curve. Rather than displaying an oscillatory behavior, the noise power shows a flat plateau at low frequencies, and falls off as $1/f^n$ at high frequencies. Except in some unusual circumstances which we will discuss elsewhere, the exponent $n \cong 1$.

A noise spectrum of the form described is predicted for the opposite geometric limit, $2\pi L/d \gg 1$, Eq. (9). Another χ^2 minimization program for Eq. (9) was applied to our data, using $W(0)$ and f_d as adjustable parameters. This fit is represented by the solid curve in Fig. 1. A good fit was obtained; however, the critical frequency, f_d^{fit}, obtained from this fitting procedure is much higher than the critical frequency calculated from either $f_d^{calc} = V_{dc}/Bd^2$, or $f_c^{calc} = V_{dc}/BdL$. Table II lists the values of f_d^{calc}, f_c^{calc}, and f_d^{fit} for the three spectra shown.

From the data in Table II, it is clear that processes corresponding to shorter times than those associated with uninterrupted flux transit across the sample width are contributing to the measured flux-flow noise. It was this result which lead us to develop a model in which moving fluxoids have their motion interrupted by pinning centers along their path.[21,23] As noted, this model leads to a spectrum as given by Eq. (11). If one assumes a distribution function so that all subpulse times up to τ_c are equally probable, i.e., $\beta = 0$, $\alpha = 1$, in Eq. (15), one can again fit the resulting spectrum to the data using a χ^2 minimization procedure. The resulting curve is indistinguishable from the solid curves shown in Fig. 1. However, the critical frequency f_c^{fit} obtained by this fitting procedure is now much less than f_d^{fit}, as can be seen by the values listed in Table II. For the annealed sample f_c^{fit} is very close to f_c^{calc}, while for the other two samples $f_c^{calc} < f_c^{fit}$.

This latter discrepancy suggests that an equally probable distribution for subpulse times up to τ_c is incorrect for samples 6*de* and 6*ne*. We, therefore, fit a large number of our spectra to Eq. (16), using $W(0)$, f_c, α, and β as adjustable parameters. When such a fitting procedure is used, we find $f_c^{fit} = f_c^{calc}$ to within the accuracy of our data, $\beta < 0.01$, and α varies from sample to sample. Because of the good agreement between the calculated and experimental critical frequencies obtained in this manner, we subsequently assumed that the critical frequency was as calculated, and varied only the three parameters α, β, and $W(0)$. Values for α obtained from the three spectra shown in Fig. 1 are given in Table II.

Following this procedure it is obvious that the high-frequency falloff in the noise is determined not only by the critical frequency (i.e., by the average transit time for fluxoids to traverse the sample) but also by the maximum duration of subpulses, and both quantities are required to characterize a spectrum. Nevertheless, in certain instances a convenient way to display data is in terms of a single parameter, F_c, which is the frequency value at which the noise power falls to the same fraction of its value at $f = 0$ as would be the case if $\alpha = 1.0$ (i.e., F_c is equivalent to f_c^{fit}). Since for $\alpha = 1.0$, $W(f_c)/W(0) = 0.45$, F_c is defined by

$$W(F_c) = 0.45\ W(0)\ ,$$

which requires that

$$F_c = f_c/\alpha\ . \tag{15}$$

In order to make comparisons between the different samples, spectra were taken on all samples at a field of 3200 Oe. On individual samples, spectra were taken at other fields, but generally in the midfield range. When averaged over all spectra for a given sample, we find $F_c > f_c$, or $\alpha < 1$. The extent by which F_c exceeds f_c is a measure of the extent to which pulses of longer duration are absent. In Table III we list for all our samples the value of α averaged over all spectra for a given sample. In obtaining this average we have omitted those spectra representing the lowest velocities. This was done because at low velocities, we are unable to measure a sufficient extent of the plateau region to obtain an unambiguous fit to the data. We have also neglected possible dependencies

TABLE III. Measured values of α for each sample.

Sample	Average of measured values of α	Standard deviation in α[a]	Number of spectra used
6*d*	0.48	±0.10	12
6*de*	0.37	±0.10	5
6*dea*	1.04	±0.35	24
6*ne*	0.72	±0.24	25
6*new*	0.75	±0.35	18
6*we*	0.28	±0.09	17
6*wec*	0.22	±0.04	3
6*te*2	0.71	±0.28	14
6*tea*	0.78	±0.50	10

[a]Assumes no field dependence of α. See text.

of α on V_{dc} and B, as we will subsequently discuss. A total of 130 spectra were used to obtain the α values for the nine samples listed in Table III.

As is obvious from Table III, values of α depend upon the sample and the sample condition. Specifically, if one follows the values of α from sample 6*de* to 6*dea* as the same sample undergoes annealing, the value of α increases from 0.37 in 6*de* to 1.04 in 6*dea*. This corresponds to a shift in the distribution function of subpulses such that after annealing, pulses up to a duration slightly larger than the average transit time across the sample are included. This shift to a preponderance of longer subpulse times can be explained in terms of the change in the grain structure with annealing at 260 °C. Electron micrographs were obtained of the surfaces of two unannealed samples 6*we* and 6*ne* using a scanning electron microscope. In both samples the grains are randomly distributed in orientation as well as in size, with the average grain size being ~30 μm. Etch pits are also observed on the surface, presumably due to preferential etching at dislocations. After annealing for one week at 260 °C, the grains grow markedly and become almost an order of magnitude larger. Etch pits are no longer observed in the surface, and we found it considerably more difficult to prepare the sample so that grain boundaries could be observed. Examination of annealed sample 6*dea* revealed grains varying from 100 to 300 μm. If, as seems likely in these samples, pinning occurs principally at grain boundaries, then subpulse times will grow longer as the distance between grain boundaries increases with annealing, and, as observed, α values increase.

Further insight into the variation of α from sample to sample can be obtained by considering the sample widths. Assuming that the various unannealed (but etched) samples have the same distribution of pinning centers, then α values should scale inversely as the sample widths. This is because a subpulse of a certain duration will represent a smaller fraction of the average flux transit time for longer transit times. Since the sample widths are 0.414 cm (6*de*), 0.198 cm (6*ne*), 0.794 cm (6*we*), one would expect $\alpha(6de)/\alpha(6ne) = 0.48$ and $\alpha(6we)/\alpha(6ne) = 0.25$. From Table III we find $\alpha(6de)/\alpha(6ne) = 0.51$ and $\alpha(6we)/\alpha(6ne) = 0.39$. The agreement in either case is well within the standard deviations for the α's. Although we unfortunately did not take detailed critical current curves for our samples, we note from limited data that the volume pinning force in sample 6*ne* was somewhat greater than in sample 6*we*. This suggests a higher density (closer spacing) of pinning centers in 6*ne* than in 6*we* and could easily account for the fact that the experimental ratio of the α's for these two samples is higher than calculated from the width ratio. On the other hand, the α's for samples 6*de* and 6*te*2 are not comparable, as might be expected from their nearly equal widths. However, sample 6*te*2 is more than twice as thick as 6*de* and the other samples. It is therefore possible that the relative role of surface and volume pinning is different in 6*te*2 from that in the other samples, and this may be responsible for the difference in the α's.

In concluding this subsection, we note that measurements on sample 6*ne* were repeated using voltage leads four times the diameter of the normal leads (sample 6*new* in Table I). Spectra taken in this configuration reproduced those taken with the narrow leads, within the general limitations of the reproducibility of our spectra in two different runs without changing the voltage leads, and we conclude that spectra are independent of the voltage probe diameter. Also, after spectra were taken on sample 6*we*, the voltage probes were moved to the center line of the sample and spectra were retaken, 6*wec*. β values remained vanishingly small while values of α and

$W(0)$ showed only slight variations between the two configurations, which also were well within the limits of the reproducibility of our spectra in two different runs. As noted in Sec. I, this suggests that edge effects do not change the character of our noise.

B. Dependence of subpulse distribution on fluxoid velocity

Implicit in the good agreement between our model and the experimental noise power spectra, as discussed in Sec. IV A, is the identification of the noise power critical frequency with the inverse of the transit time as calculated from Eq. (5). Since the critical frequency increases in proportion to the fluxoid velocity, f_c will increase in proportion to the ratio V_{dc}/B.

In our model the frequency dependence of the spectrum is determined by a combination of f_c and the length of the times between pinning events. If the number of pinning centers which are effective in interrupting flux motion increases or decreases with increases in the Lorentz driving force, $\vec{J} \times \vec{B}$, or separately on changes in V_{dc} or B, this should result in a shift in the distribution function $g(\tau_i)$ so as to include a lesser or greater proportion of long pulses. In order to determine if such shifts are occurring, we have studied the dependence of F_c on fluxoid velocity. A linear dependence of F_c on velocity for a given sample implies that the same distribution of subpulse times, and hence the same distribution of effective pinning centers, exists, independent of the dc voltage level or magnetic field.

In Fig. 2, we plot F_c vs V_{dc} at the constant magnetic field of 3200 Oe for samples 6*d*, 6*de*, and 6*dea*, and in Fig. 3 similar data for sample 6*ne* at three different fields. The linear dependence of F_c on V_{dc} is clearly demonstrated and the solid lines in the figures represent a linear least-square fit to the data. Our results therefore indicate that at a fixed field, this distribution of effective pinning sites is independent of fluxoid velocity or Lorentz driving force.

We note that in the three cases shown for the 6*d* series, $F_c = 2.1 f_c$ (as prepared), $F_c = 2.7 f_c$ (etched), and $F_c = 1.0 f_c$ (annealed). It is somewhat surprising that etching increases F_c, since it reduces the critical current, and hence one would also assume, the density of surface pinning centers. We have no explanation for this result, but note that the relative role of surface and volume pinning has previously been the subject of different interpretations, and is still not well understood.

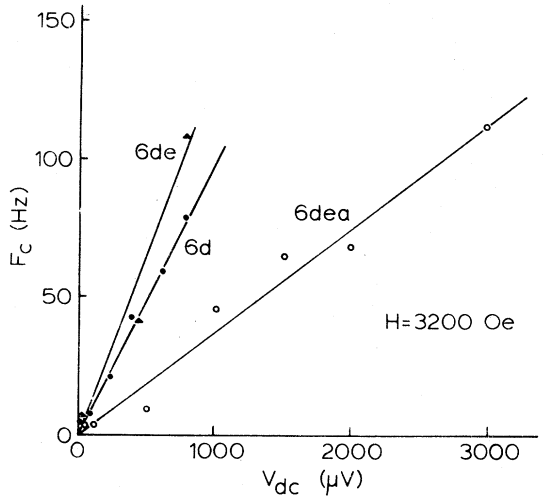

FIG. 2. F_c vs V_{dc} for samples 6*d* (unetched and unannealed), 6*de* (etched and unannealed), and 6*dea* (etched and annealed). Data shown are taken at $H = 3200$ Oe, $T = 2.14$ K. The solid lines represent least-square fits to the data. The linear relationship between F_c and V_{dc} implies that α is constant and that the distribution function for the duration of subpulses is not a function of voltage.

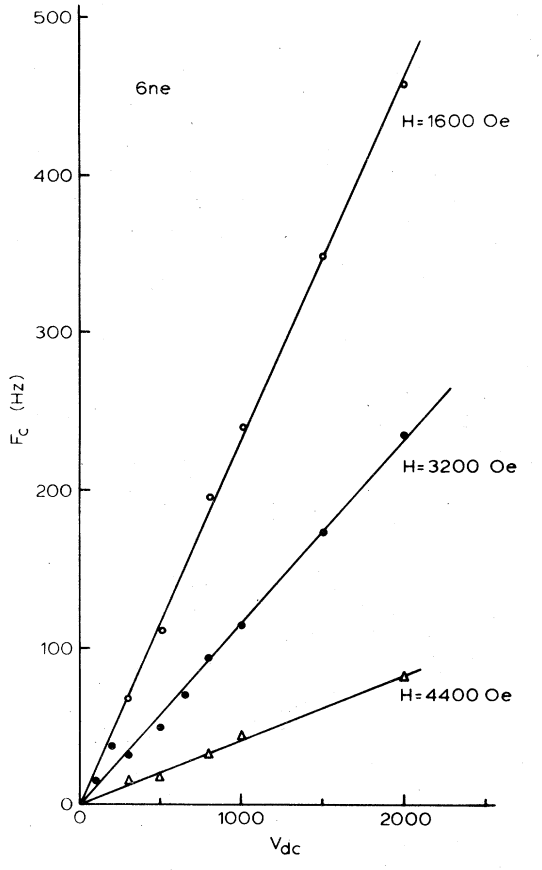

FIG. 3. F_c vs V_{dc} for unannealed, etched sample, 6*ne*, for fields of 1600, 3200, and 4400 Oe. $T = 2.14$ K. Solid lines represent least-square fit to the data. Data demonstrate that for a fixed voltage, the critical frequency decreases with increasing field.

In order to test the linearity of F_c on $1/B$, one could measure F_c at a constant voltage and vary the field. Plots of such data usually show considerably more scatter than plots of F_c vs V_{dc}. Also, it was not always convenient to take measurements at the same voltage levels for different fields. Thus, we used plots of F_c vs V_{dc} at constant field, like those of Figs. 2 and 3, in order to determine the slope $(\partial F_c/\partial V_{dc})$, and plotted the results as a function of $1/B$. In Fig. 4 we have shown the results for sample 6*ne*. The error bars on the points represent the standard deviations in the values of F_c/V_{dc} for different values of V_{dc} at a fixed field. A monotonic increase of F_c with $1/B$ clearly occurs, but the expected linear dependence does not seem to be present. In fact, for those samples in which sufficient data exist to draw a conclusion, points in the midfield range lie above the solid line drawn assuming a constant average α, while points at high and low fields appear to lie below the line.

The latter results suggest that α is not constant as a function of field. This can be seen more clearly in Fig. 5 where we have plotted α values averaged at a given field as a function of B. It can be seen in Fig. 5 that α goes through a minimum in the midfield range where the volume pinning force goes through a maximum, and the mechanism for initiating flux-flow changes from pin breaking to shear.[32] Generally this minimum appears to be less pronounced after annealing, although we emphasize that the present data is not sufficiently extensive nor precise to draw more than the general conclusions made thus far. A careful study of the field dependence of α correlated with a study of the field dependence of the volume pinning force would seem worthwhile.

To summarize, for a *fixed* field there does not seem to be a relative shift in the distribution function of subpulses with increasing Lorentz force or increasing fluxoid velocities. There is an *absolute* shift in the distribution as τ_c decreases with increasing V_{dc} so that α remains constant. α does not appear to remain constant, as a function of magnetic field, although F_c does increase monotonically with $1/B$. The relatively large standard deviations accompanying the α values in Table III are calculated assuming α is independent of B, and therefore reflect this apparently incorrect assumption.

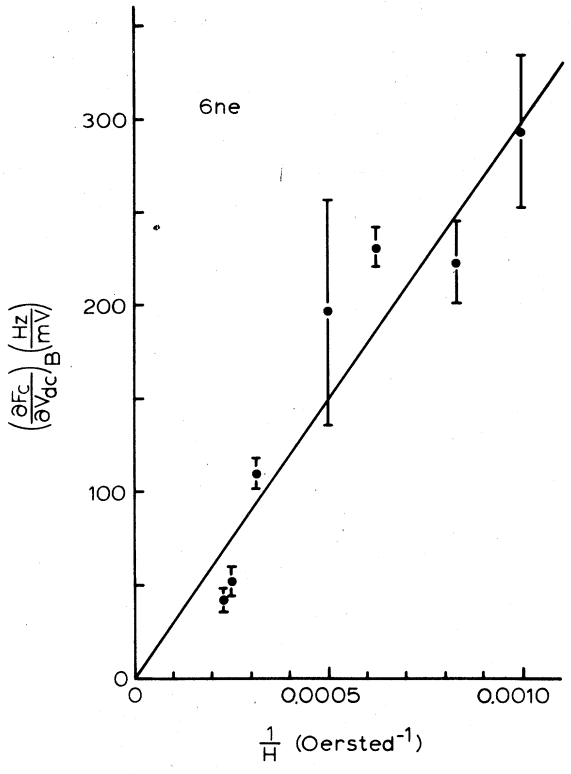

FIG. 4. Relation between $(\partial F_c/\partial V_{dc})_B$ and $1/H$ for sample 6*ne*. $(\partial F_c/\partial V_{dc})_B$ is obtained from plots of F_c vs V_{dc} at constant field like those of Fig. 3. The error bars on the points represent standard deviations in values of F_c/V_{dc} for different values of V_{dc} at fixed field. The solid curve represents a least-square fit for the predicted linear dependence.

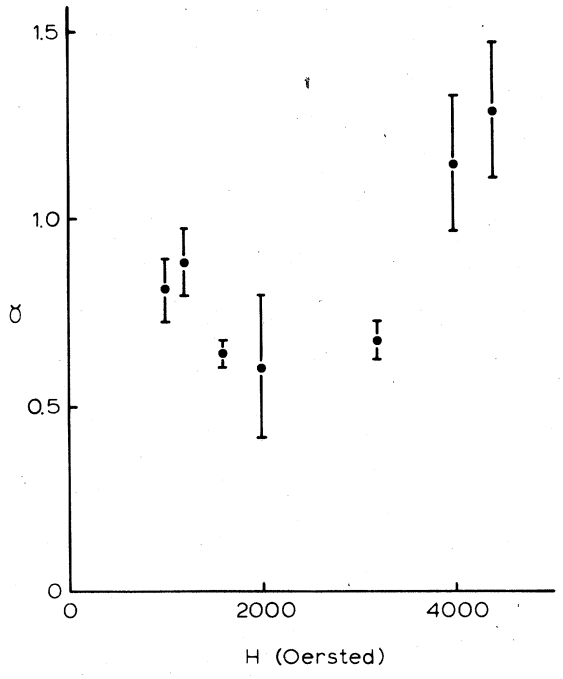

FIG. 5. α vs H for sample 6*ne*. Data show that α goes through a minimum in the midfield range where the volume pinning force displays a broad maximum.

C. Effects of field, dc voltage, fluxoid velocity, and Lorentz force on generalized flux bundle size

Although, as we have noted, our recent model of flux flow indicates that it is not possible to extract intrinsic flux bundle size directly from the noise power extrapolated to zero frequency, it is still of interest to deal with the noise power normalized by the dc voltage. This is because the resulting quantity, which we shall refer to as the "generalized flux bundle size", contains parameters of interest. We thus define the generalized flux bundle size as

$$n(0)=\frac{W(0)}{2\phi_0 V_{\rm dc}}=\frac{\langle\Phi^2\rangle\langle l^2\rangle}{\phi_0\langle\Phi\rangle\langle l\rangle L}\ , \tag{16}$$

where ϕ_0 is the elementary flux quantum. Thus defined, $n(0)$ would represent the flux bundle size in earlier models in which $\langle l\rangle=\langle l^2\rangle^{1/2}=L$, and all flux bundles are assumed to be of equal size. We note that if bundles are all the same size, there would be a noise reduction in our model proportional to $\langle l^2\rangle/\langle l\rangle L$ as compared to the earlier models. We also note that in neither case is the possibility of noise reduction by long-range correlation explicitly included.

It is possible to study $n(0)$ as a function of magnetic field, dc voltage (or current), or the product variables representing fluxoid velocity, E/B, and Lorentz force, $\vec{J}\times\vec{B}$. In order to carry out such studies we have used the 130 complete spectra which were used to study frequency effects. In addition, to obtain a more complete picture of the functional variation of the generalized bundle size, we have obtained values of $n(0)$ using "partial spectra". A partial spectrum is a noise power measurement taken at a low frequency, usually 10 Hz, and a single higher frequency. The higher-frequency measurement is used to establish a consistency of the partial spectrum with complete spectra taken at other values of field or voltage. The 10 Hz measurement is used to approximate the noise at zero frequency. Because of the flat plateau in the noise spectra at low frequencies, generally $\delta V^2(f=10)\approx\delta V^2(f=0)$ with minimal error, except in those cases where the average fluxoid velocity is so low that the plateau region is not well established.

In Fig. 6, we show plots of $n(0)$ versus voltage at the constant magnetic field, $H=3200$ Oe, for samples 6*d*, 6*de*, and 6*dea*. At lower voltages $n(0)$ initially decreases exponentially with voltage (and hence with average velocity for constant field), and then at higher voltages falls off more slowly. The exponential dependence covers the nonlinear flux-flow region. In addition, we note that at $V_{\rm dc}=0$, etching reduces $n(0)$ somewhat, but subsequent annealing of the sample increases $n(0)$ significantly.

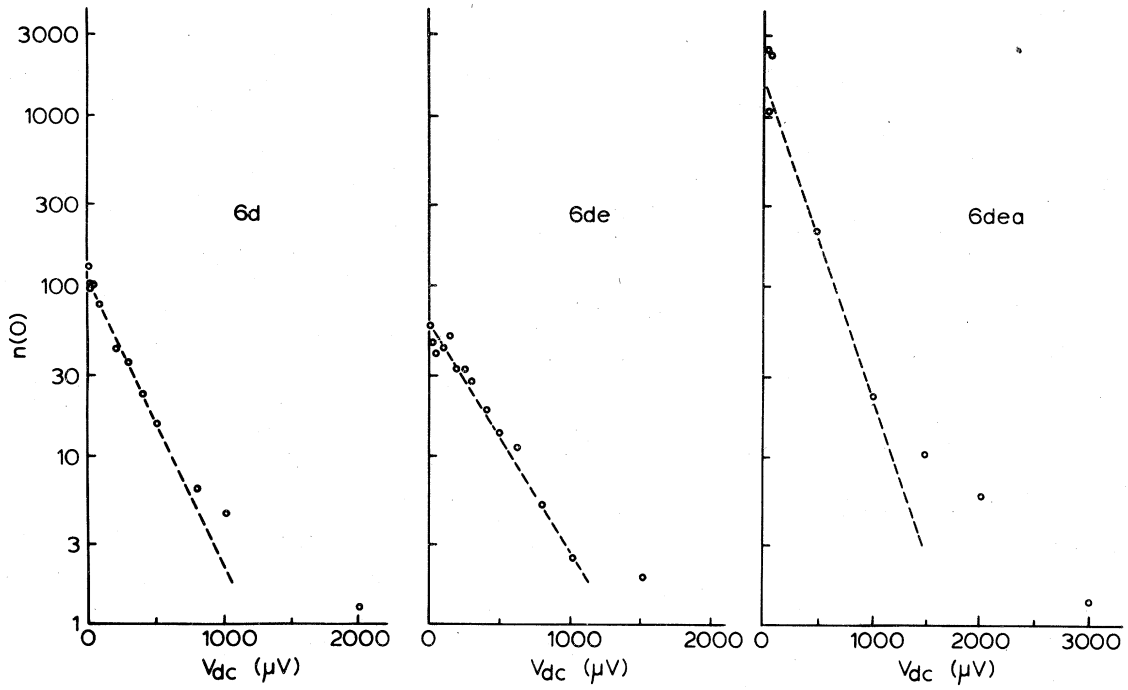

FIG. 6. Generalized flux bundle size, $n(0)$, as a function of dc voltage for samples 6*d* (unetched and unannealed), 6*de* (etched and unannealed), and 6*dea* (etched and annealed). $H=3200$ Oe, $T=2.14$ K. Data demonstrate that annealing greatly increases the bundle size at low velocity.

The reason for the observed voltage (velocity) dependence of $n(0)$ is not obvious. Further insight may perhaps be obtained from plots like those of Fig. 7, where we show for a constant field the relationship between $n(0)$ vs J (hence Lorentz force), for sample 6*d*. In such a plot we find that $n(0)$ decreases exponentially with J even at current values where the exponential dependence of $n(0)$ on V is no longer obtained. This suggests that the dependencies observed in both kinds of plots are a result of an exponential decrease of $n(0)$ with the Lorentz force (at constant field). We suggest further that this decrease in $n(0)$ results from a decrease in the average intrinsic flux bundle size with increasing Lorentz force. At low currents many fluxoids have not been set in motion. These immobile fluxoids should act as barriers, impeding the motion of other groups of fluxoids which have overcome local pinning forces. Therefore, one would expect that in this situation $\langle l^2\rangle/\langle l\rangle L$ would be smaller than would be the case at higher currents where most of the fluxoids are in motion. Since we expect that this ratio should increase with J, at least into the linear flux-flow region, the decrease in $n(0)$ must be attributed to a decrease in the ratio $\langle\Phi^2\rangle/\langle\Phi\rangle$ with increasing J.

We have also noted an interesting relationship for the total noise $\langle\delta V^2\rangle_{f=0}$ as a function of voltage at constant magnetic field. In Fig. 8 we have plotted $\langle\delta V^2\rangle$ vs $v = V_{dc}/Bd$ at two different fields for sample 6*d*. The shape of the curve suggests a resonant effect whereby fluxoids might be moving between pinning centers of fixed separation (or moving across the entire sample) at some preferred rate. This suggested that if an ac current signal were applied, and the frequency of this signal were swept, that a resonant voltage might be detected at an appropriate frequency. No such effect was observed. We, therefore, are now inclined to believe that the maximum in the noise is the "accidental" result of the functional dependencies described above. Since at low velocities, we have shown $n(0) = ae^{-bV_{dc}}$, where a and b are constants depending on magnetic field, and

$$\langle\delta V^2\rangle = 2n(0)\phi_0 V_{dc} = 2\phi_0 a V_{dc} e^{-bV_{dc}}$$

the functional dependence for the noise at zero frequency requires that there should be a maximum at $V_{dc} = 1/b$. The shifting of the noise peak to lower velocities as the field increases, as is apparent in Fig. 8 is consistent with values of b obtained from exponential plots of $n(0)$ vs V_{dc} for different field values.

We conclude this section by showing in Fig. 9 curves of $n(0)$ vs B for different values of V_{dc}. The form of the magnetic field dependence of $n(0)$ is obviously a strong function of the dc voltage level. Be-

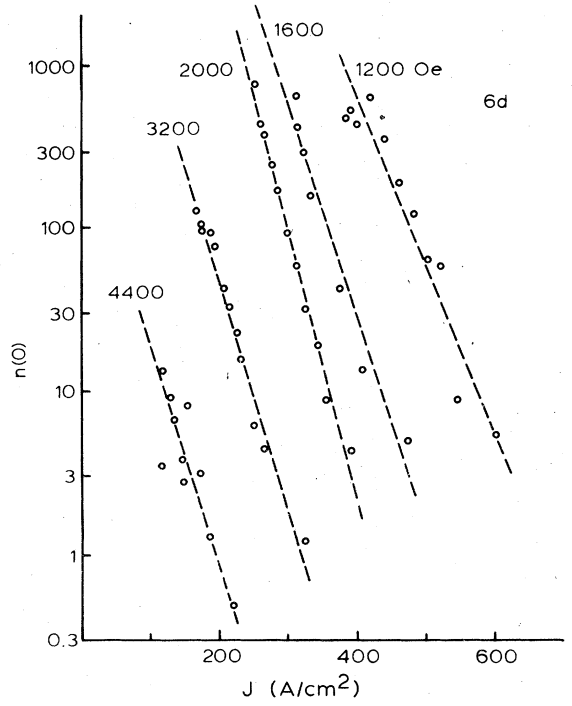

FIG. 7. Generalized flux bundle size, $n(0)$, as a function of transport current density, J, for sample 6*d* at various magnetic fields. $T = 2.14$ K.

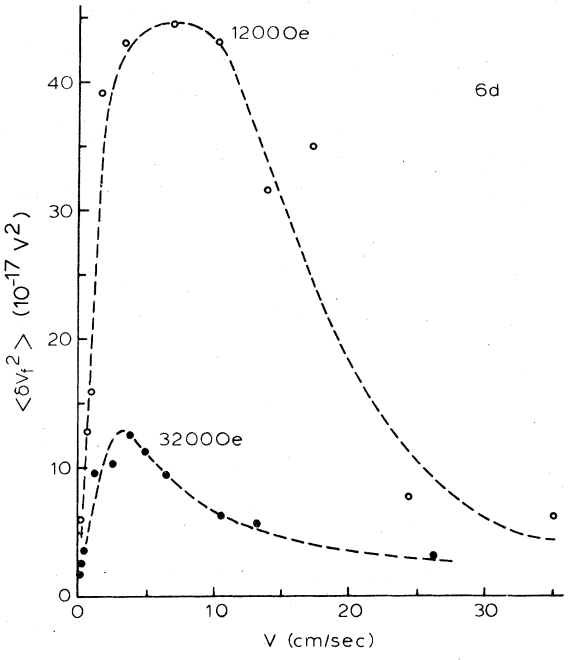

FIG. 8. Mean-square noise voltage at a frequency of 10 cycles, $\langle\delta V^2(f=10)\rangle$ as a function of average fluxoid velocity for constant fields of 1200 and 3200 Oe. Sample is 6*d*. The dashed curves serve only to delineate the data points.

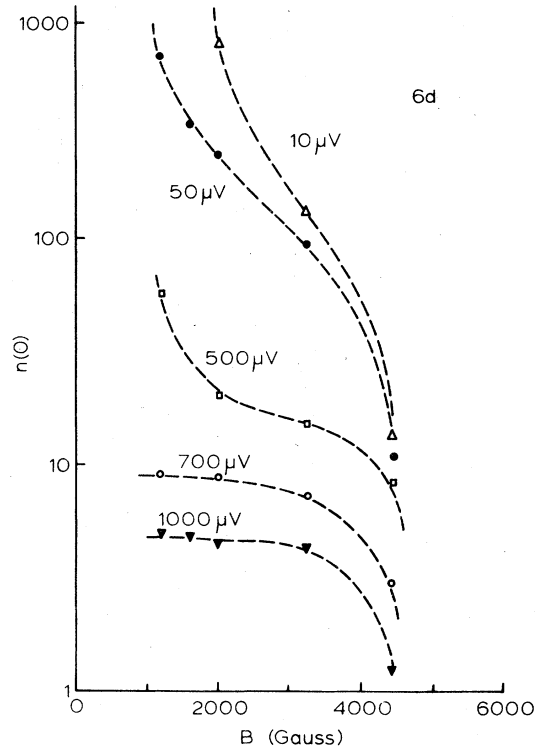

FIG. 9. Generalized flux bundle size, $n(0)$, vs magnetic field for sample 6*d*, and using various dc voltage levels as shown. Because the spectra have not plateaued at the frequencies of measurement when V_{dc} is small, the 10- and 50-μV data may be inaccurate. The dashed curves are shown only to delineate the data for the different voltages.

cause the data obtained at low dc voltages does not satisfy the criterion $\delta V^2(f=10) \cong \delta V^2(f=0)$, the data at 10$\mu$V and 50$\mu$V may not be an accurate reflection of the magnetic field dependence of $n(0)$. Nevertheless, at all voltages there is a rapid decrease in the noise at high fields, and more specifically, for the sample shown this falloff begins at approximately 3200 Oe. The critical volume pinning force curve for this sample shows a very broad force peak centered at approximately 3200 Oe.

The force peak has generally been attributed to a transition from flux flow initiated by pin breaking to flux flow initiated by shear.[32] The latter mechanism occurs at a field where the elastic shear constant c_{66} has become sufficiently reduced so that weakly pinned fluxoids are able to shear around more strongly pinned fluxoids. Thus, instead of a larger group of fluxoids becoming simultaneously depinned, smaller groups begin moving by shear. We suggest that the generalized bundle size reduction at high fields as shown in Fig. 9 results from this mechanism. Preliminary work on samples with other shapes to the critical force curves gives support to this suggestion.

D. Effects of metallurgical condition

The metallurgical state of our samples was changed in two ways: (a) a sample which had been cold worked and left at room temperature for a day, (6*d*), was etched to remove surface damage, (6*de*); (b) the same sample was subsequently annealed for one week at a temperature of 260 °C, (6*dea*). The surface of the etched sample exhibited a number of etch pits, indicating the presence of dislocations, and showed a distribution of grain sizes with an average size of 30 μm. After annealing, the average grain size grew by an order of magnitude to 100–300 μm. After annealing, etching did not produce etch pits.

The noise measurements used for detailed comparisons between the samples were made at only one field value, 3200 Oe. This is unfortunate, because, as noted above, we have subsequently obtained preliminary indications from other samples that noise changes with field depend upon the shape of the curve of volume pinning force versus field. Our results, showing $n(0)$ vs V_{dc} for the fixed field of 3200 Oe, were displayed in Fig. 6. Etching reduces the critical current, and hence the value of the volume pinning force, by a factor of three. However, the flux bundle size is reduced by a factor of only about 40% for voltage (or velocity) extrapolated to zero, and by a smaller factor at higher velocities. Since etching affects only the surface metallurgy, the critical current decrease must result from a decrease in the surface pinning. On the other hand, since there was only a relatively smaller decrease in the noise upon etching, it appears that the generalized bundle size is determined primarily by interactions with pinning centers in the bulk. It is interesting to note that generalized bundle sizes of several etched samples made from the same ingot were approximately of the same magnitude as displayed in Fig. 6 for sample 6*de*. Becuase these samples did come from the same ingot, their bulk metallurgical structures should have been approximately the same. However, the surfaces of these other samples obviously differed, as was apparent from the measured variations in their critical currents. We therefore take this as further evidence that bundle sizes are primarily determined by the bulk pinning centers.

After the sample is annealed, there is a large increase in the generalized bundle size as can be seen by comparing data from samples 6*de* and 6*dea* in Fig. 6. Again, the difference is most pronounced at low velocities. At $v=0$, the bundle size after annealing has increased by a factor of approximately 25. Surprisingly, annealing approximately doubles the critical current as grain sizes increase from 30 μm to 100–300 μm. We have already noted that as the grain size increases, the frequency distribution of the noise shifts so as to include larger subpulse times. We now observe higher values of $n(0)$ as the grain

size increases, and we believe it is reasonable to attribute both effects to the increased grain size.

Since several factors are included in the expression for the generalized bundle size, it is not possible to present an unambiguous model for determining the flux bundle size from the grain diameter. We note, however, that the typical spacing between fluxoids at the field of measurement is approximately 10^{-5} cm. For the unannealed foil with a 30-μm average grain diameter, if we aligned a single row of fluxoids along a grain boundary, approximately 300 fluxoids could be accomodated. Assuming that the generalized bundle size, $n(0)$, is equal to the intrinsic bundle size, $\langle\phi\rangle/\phi_0$, the noise amplitude (at $v=0$) would give a bundle size of approximately 100 fluxoids. The difference between these numbers could then be attributed to the other factors contained in the expression for $n(0)$. Since annealing increases the grain size as noted above, then according to the model of a flux bundle just described, in an annealed sample one would expect a grain boundary to accomodate 1000 to 3000 fluxoids. The bundle size observed at $v=0$ for sample 6*dea* in Fig. 6 fits within this range.

From this model we are led to the concept of a "flux bundle" not as a cluster of fluxoids, but as an extended line formed by pinning along a grain boundary or other lattice imperfection, and which then moves as a unit across the grain boundary once the pinning interaction has been overcome. This leads to a qualitative understanding of the noise reduction which accompanies larger Lorentz driving forces or higher fluxoid velocities. As we have noted, the distribution of subpulse times depends on metallurgy, but at constant field it does not depend on the driving force or velocity. A pinning center which interrupts fluxoid motion at low velocities is also effective in interrupting fluxoid motion at high velocities (since α and β are independent of velocity). It is not likely, therefore, that changes in bundle size accompanying changes in velocity can be attributed to the change in active pinning centers.

We therefore offer as a tentative model of fluxoid motion the idea that in the present samples "flux bundles" are defined by interactions with grain boundaries. These grain boundaries temporarily interrupt the motion of the moving fluxoids until all those fluxoids aligned along a boundary move across the boundary as a unit. Grain boundaries are aligned randomly with respect to the macroscopic Lorentz force, but the boundary pinning provides a local resistanceless current path, and this local force pushes the fluxoids perpendicularly across the boundary. Within the grain, fluxoids travel parallel to the macroscopic Lorentz force, but near the grain boundary, the velocity field alters its direction and becomes perpendicular to the boundary. A flux bundle may, therefore, be defined as that group of fluxoids with the same velocity field. At low velocities, and smaller driving forces, those fluxoids overcoming pinning at a boundary will travel some distance into the grain before their velocity becomes parallel to the driving force, but as the force and velocity become larger, this distance will become less. As fluxoids travel across a greater portion of the grain with the same velocity, long-range correlation becomes an important determinant of the noise amplitude, and thus noise reduction takes place.

We have in the presentation of this model completely ignored other factors appearing in Eq. (16), and which presumably also determine the noise level. In particular, one would expect changes in the factor $\langle l_i^2\rangle/\langle l_i\rangle$ on annealing to contribute to enhanced noise. In fact, if we were to assume that $\langle\phi\rangle$ remained unchanged on annealing, the change in $n(0)$ could be accounted for rather well by the increase in this ratio. However, in the present case, the distance over which fluxoid motion is correlated is also proportional to grain size, and this factor might be able to produce a noise reduction tending to cancel out the noise increase anticipated with larger l_i.

VI. SUMMARY

The present work demonstrates that experimental flux-flow noise spectra can be fit using a model of fluxoid motion interrupted by pinning centers. A new frequency $F_c = f_c/\alpha$ is introduced, where α is a fitting parameter such that $\alpha\tau_c$ measures the longest times present in the distribution of subpulses. From our measurements we conclude that α has the following properties: (i) α depends on sample condition, with annealing and larger grain size producing larger values of α; (ii) α appears to scale approximately inversely with sample width for samples having the same metallurgical history, provided their surface to volume ratios are also equal; (iii) α does not change with velocity or Lorentz force (i.e., J or V_{dc}) when the magnetic field is fixed, suggesting that if a pinning center exists, it is effective in interrupting flux motion at all velocities and forces within the range measured; and (iv) α goes through a minimum in the field range where the volume pinning force goes through a maximum, even though F_c increases monotonically with $1/B$.

Our model of flux motion interrupted by pinning centers leads to the result that the noise magnitude at zero frequency divided by dc voltage is not simply proportional to the average flux bundle size, but is determined by other factors including averages of distances between pinning events. We introduce the concept of the generalized flux bundle size, $n(0)$, to include all these factors. We find that $n(0)$ has the following properties: (i) $n(0)$ at a fixed field decreases exponentially with Lorentz force over the current range used (i.e., it is exponential in J rather

than V_{dc}); (ii) $n(0)$ falls off at high fields with the falloff beginning in the field range where the force peak occurs; (iii) $n(0)$ can be changed by metallurgical treatment, and in particular, annealing, which produces larger grain sizes, increases $n(0)$. We suggest that this latter result can be understood from our model either in terms of lengthening the distance between pinning events, or in terms of increasing the width of the barrier to the flux motion.

We have also observed a maximum in the flux-flow noise as a function of velocity (at constant field) which we conclude is not related to a resonance in the flux motion, but is the consequence of the proportionality of the noise magnitude to V_{dc} and to the exponential decrease of the noise with velocity referred to above.

These results lead us to conclude that the concept of a flux bundle arises only because of the existence of pinning centers which change the velocity field of a group of fluxoids and give them an identity different from that of the other fluxoids.

The relationship between the flux-flow noise and the pinning suggests that more detailed measurements relating the noise spectra to volume pinning force curves would be of considerable interest.

ACKNOWLEDGMENT

We wish to acknowledge the early support of this research by the Research Corporation and the current support by DOE under Contract No. DOE 76-S-02-2890. We are also appreciative of the help given us by Professor John Moteff in characterizing the grain boundary sizes in our samples.

---

*Present address: Los Alamos Scientific Laboratory.

[1]U. Essmann and H. Trauble, Phys. Status Solidi 18, 813 (1966).

[2]U. Essman and H. Trauble, J. Appl. Phys. 39, 4052 (1968).

[3]N. V. Sarma, Phys. Lett. A 25, 315 (1967).

[4]D. Cribier, Phys. Lett. 9, 106 (1964).

[5]J. Schelten, H. Ullmaier, and W. Schmatz, Phys. Status Solidi B 48, 619 (1971).

[6]P. R. Solomon, Phys. Rev. 179, 475 (1969).

[7]J. Schelten, H. Ullmaier, and G. Lippman, Phys. Rev. B 12, 1772 (1975).

[8]D. M. Kroger and J. Schelten, J. Low Temp. Phys. 25, 369 (1976).

[9]D. J. van Ooijen and G. J. van Gurp, Phys. Lett. 17, 230 (1965).

[10]G. J. van Gurp, Phys. Rev. 166, 436 (1968).

[11]R. E. Burgess, Physica (Utrecht) 55, 369 (1971).

[12]J. R. Clem, Phys. Rev. B 1, 2140 (1970).

[13]J. R. Clem, Physica (Utrecht) 55, 376 (1971).

[14]J. B. Kruger and C. Heiden, *Proceeding of the 12th International Conference on Low Temperature Physics, Kyoto, 1970,* edited by E. Kanda (Academic, Tokyo, 1971), p. 415.

[15]C. Heiden and H. P. Friedrich, Solid State Commun. 9, 323 (1971).

[16]C. Heiden, *Low Temperature Physics LT 13,* edited by K. D. Timmerlous, W. J. O'Sullivan and E. F. Hammel (Plenum Press, New York, 1974), Vol. 3, p. 75.

[17]C. Heiden and D. Kohake, Phys. Status Solidi B 64, K83 (1974).

[18]C. Heiden, Solid State Commun. 18, 253 (1976).

[19]P. Jarvis and J. G. Park, J. Phys. F 4, 1238 (1974).

[20]P. Jarvis and J. G. Park, J. Phys. F 5, 1573 (1975).

[21]J. Thompson and W. C. H. Joiner, Solid State Commun. 16, 849 (1975).

[22]F. Habbal and W. C. H. Joiner, Phys. Lett. A 60, 434 (1977).

[23]F. Habbal and W. C. H. Joiner, J. Low Temp. Phys. 28, 83 (1977).

[24]A. van der Ziel, Phys. Lett. A 25, 672 (1967).

[25]S. W. Shen, Appl. Phys. Lett. 17, 415 (1970).

[26]S. W. Shen and A. van der Ziel, Physica (Utrecht) 64, 587 (1973).

[27]H. M. Choe and A. van der Ziel, Physica (Utrecht) B 81, 237 (1976).

[28]J. M. A. Wade, Philos Mag. 23, 1039 (1971).

[29]J. R. Clem, *Noise in Physical Systems, Proceedings of the Fifth International Conference on Noise, Bad Nauheim, Germany, 1978,* edited by D. Wolf (Springer-Verlag, Berlin, 1978), p. 214.

[30]J. R. Clem, J. Phys. (Paris) 39, C6-619 (1978).

[31]D. K. C. McDonald, *Noise and Fluctuations* (Wiley, New York, 1962), p. 37.

[32]E. J. Kramer, J. Appl. Phys. 44, 1360 (1973).